Dalton Transactions

An international journal of inorganic chemistry

rsc.li/dalton

Zinc binding sites in Pra1, a zincophore from *Candida albicans*†
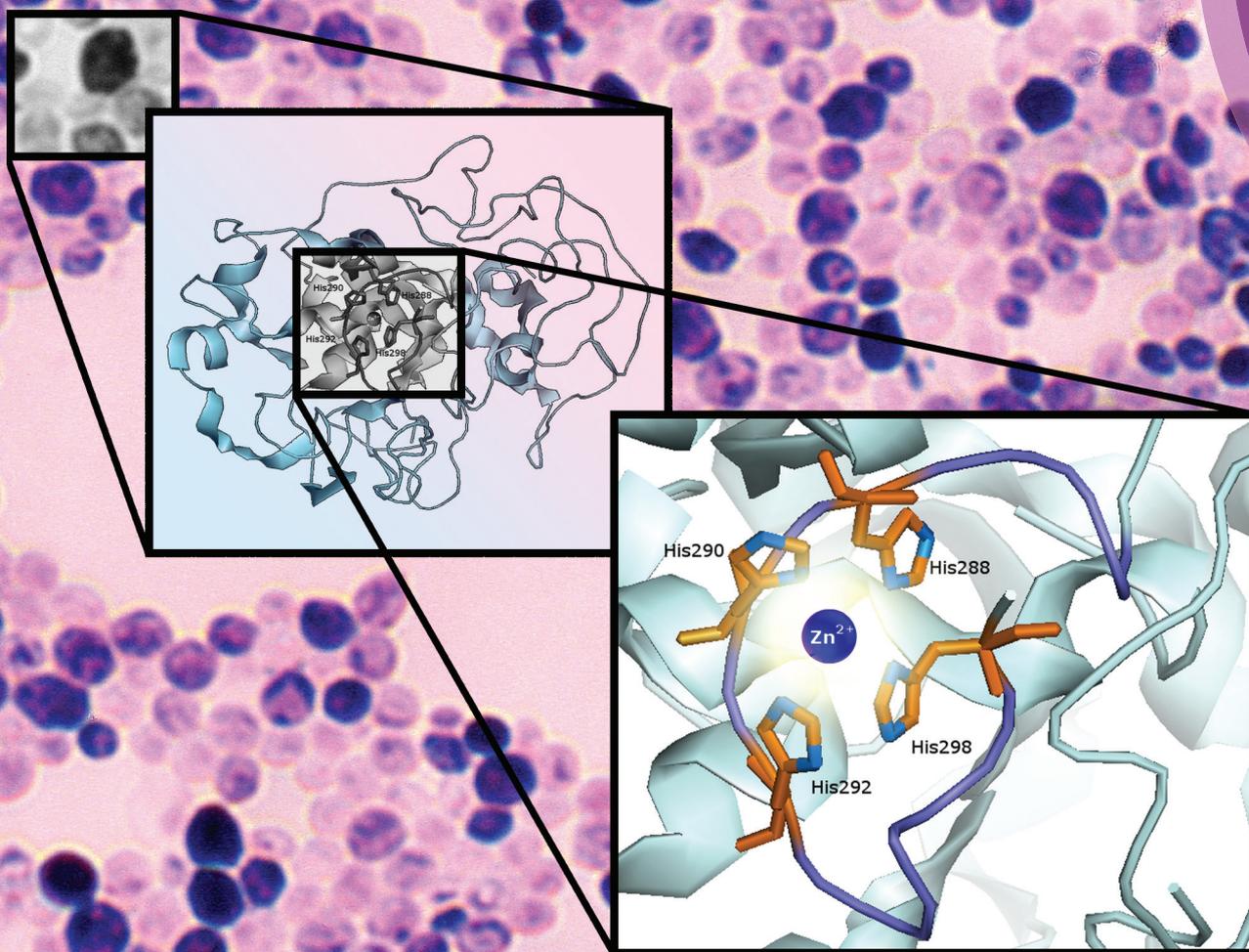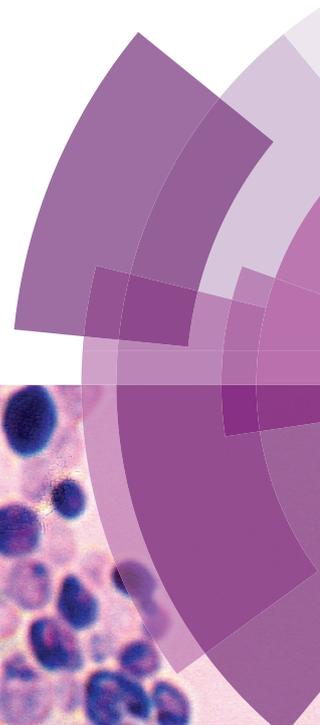
Dorota Łoboda and Magdalena Rowińska-Żyrek (ID) *

The aim of this work is to understand the interactions of Zn(II) with Pra1, a zincophore from *Candida albicans*, one of the most common causes of serious fungal infections in humans. Pra1 is a 299 amino acid protein, secreted from the fungus to specifically bind Zn(II) and deliver it to a transmembrane zinc transporter, Zrt1. We take the first step towards understanding the bioinorganic chemistry of this process, by pointing out the Zn(II) binding sites in Pra1 and understanding the thermodynamics of such interactions. Our approach involves working on model systems (unstructured parts of proteins) in order to identify those regions in Pra1, to which zinc binds with the highest affinity. Mass spectrometry shows the stoichiometry of Zn(II)–peptide complex formation and potentiometric studies give us the partial and overall stability constants for all the formed zinc complexes. NMR clarifies binding sites in the case of doubts. A detailed comparison of these results shows that the C-terminal region of Pra1 binds Zn(II) with the highest affinity, indicating that this region of the zincophore is responsible for the binding of zinc. Such knowledge is an input to the basic bioinorganic chemistry of zinc; it allows us to understand the inorganic biochemistry of zincophores, and it might be a stepping stone towards finding new, fungus specific treatments based on parts of zincophores coupled with antifungal drugs.

Introduction

Candida albicans is one of the most common fungal species of the normal human microbiome. Although it is typically a commensal of the oral cavity, and gastrointestinal and urigenitary tracts, *C. albicans* is also the most common agent of candidiasis – a condition that encompasses infections that range from superficial (such as oral thrush or vaginitis) to systemic and potentially life-threatening candidemia (invasive candidiasis), which occurs when the fungus is present not only on mucosal surfaces, but invades the bloodstream, causing infections anywhere in the body. Invasive candidiasis is usually confined to severely immunocompromised patients.[1] Mortality among patients with invasive candidiasis is as high as 40%, even when patients receive antifungal therapy.[2] The second most frequently identified fungal pathogen is *Aspergillus fumigatus*, which causes chronic, invasive and allergic forms of aspergillosis not only in immunosuppressed people, but also in patients with underlying illnesses such as tuberculosis or chronic obstructive pulmonary disease and with otherwise healthy immune systems.[3] The frequency of drug resistant invasive mycoses due to opportunistic fungal pathogens has increased significantly over the past three decades, and is becoming a serious medical problem in immunosuppressed patients. It was suggested that fungal pathogens may ultimately become a greater medical problem than drug resistant bacterial 'superbugs'.[4]

One of the biggest obstacles in finding new fungus-specific therapeutics comes from the fact that fungi share essential metabolic pathways and core cellular machineries with humans, much more than disease-causing bacteria.[5] In order to design a highly specific antifungal drug, it is crucial to understand and aim at differences in the human and fungal metabolism.[6]

Although pathogen-selective targets are scarce, there is at least one significant difference between fungal and mammalian cells: the zinc transport system based on zincophores – present in fungi, absent in humans. Zinc is an essential metal for a plethora of cellular events and therefore is an indispensable micronutrient for almost all living organisms. 9% of fungal proteomes consist of zinc-binding proteins;[7,8] a quarter of these proteins are involved in transcriptional regulation, *e.g.* being zinc finger transcription factors (116 different ones in *C. albicans* and 311 in *A. fumigatus*) or regulators of several biological processes, such as amino acid metabolism, nitrogen utilization or cell division.[9]

Numerous zinc-binding proteins are involved in fungal virulence. Superoxide dismutases (SODs) are the central enzymes in fungi associated with the detoxification of ROS generated by

Faculty of Chemistry, University of Wroclaw, F. Joliot-Curie 14, 50-383 Wroclaw, Poland. E-mail: magdalena.rowinska-zyrek@chem.uni.wroc.pl

host cells during host–pathogen interactions.[10] For this reason, specific SODs from pathogenic fungi are assumed to be virulence determinants. Also the zinc-binding metalloproteases have been shown to be involved in pathogen invasion.[11] Examples of such metalloproteases are ADAM metalloproteinases or deuterolysin (with two zinc-binding histidines and a catalytic glutamate in its catalytic centre).[12]

Beyond any doubt, Zn(II) is crucial for both virulence and survival of fungal pathogens in humans. The task of the uptake of this metal is far from being trivial, with the total host tissue zinc concentration being in the range of 11–23 μM[13,14] and the concentration of free Zn(II), not bound to the proteins of the host, is supposed to be as low as 0.1–1 nM.[15] The host organism does not make the zinc uptake easier. In fact, the infected host seems to take advantage of the essentiality of this nutrient for fungi and to hamper the pathogen growth, mammals reduce the levels of free zinc (the host restriction of microbial access to certain key nutrients is a process termed nutritional immunity).[16,17] This Zn(II) availability restriction is achieved by lowering the availability of free zinc *via* the activity of the host zinc transporters or the expression of zinc-binding proteins, such as calprotectin, a member of the S100 family of metal-binding proteins, produced by neutrophils in order to reduce the overgrowth of fungi such as *Aspergillus fumigatus* and *C. albicans.*[18–20]

Pathogenic fungi have adapted to these Zn(II)-limiting conditions imposed by the host by developing additional mechanisms to sequester zinc from host cells and tissues – they secrete specific zinc selective chelators, which bind the crucial metal ion and deliver it to the specific fungal membrane transporters. This process is analogous to the well-known iron chelation by secreted siderophores – low molecular weight iron carriers synthesised by bacteria or fungi and secreted into the environment of the host, where they bind ferric ions with high affinity and selectivity. The delivery of iron-loaded siderophores back to the microorganism occurs *via* specific membrane receptors and transport proteins. An analogous process occurs for zincophores, although the dimensions of the secreted protein, the chemical nature of the process and the mechanism of metal binding are completely different from the ones observed for siderophores.[21]

The protein based zincophore is a novelty in the scientific world. It was suggested for Pra1, a small, 299 amino acid, secreted zinc binding protein, which can take up this metal from the environment and re-associate with the fungus *via* a co-expressed, genetically-linked membrane transporter, Zrt1. Recently, Citiulo *et al.*[22] elucidated the mechanism of *C. albicans* zinc acquisition from host cells: (i) after the host cell invasion Pra1 (pH-regulated antigen 1, the previously mentioned zincophore) is expressed due to the alkaline pH and the low amount of soluble zinc of the intracellular environment;[23,24] (ii) the protein is secreted and released from the fungal cell surface, predominantly in the hyphal form; it is required for hyphal extension, but does not directly cause damage of the host; (iii) it binds host cellular zinc and (iv) returns to the fungal cell *via* a physical interaction with Zrt1, a

membrane transporter, to deliver the bound metal ion (Fig. 1).[22]

The *PRA1* and *ZRT1* genes share their upstream intergenic regions, are transcriptionally co-regulated and exhibit similar expression patterns during the invasion of oral epithelial cells. Hube's group showed that the deletion of the *PRA1* gene prevented the utilisation of host zinc and damage of host cells in the absence of exogenous zinc, showing a crucial role of this protein for pathogenicity.[22,25]

The zinc transport system seems to be very well conserved also in other fungi. Another recent study reported that two genes from *A. fumigatus*, *zrfC* and *aspF2*, share their upstream intergenic regions, are co-regulated and required for growth under zinc limiting conditions,[26,27] *e.g.*, in the presence of the Zn(II)-chelating protein calprotectin.[28]

What is most interesting is the fact that Pra1 from *C. albicans* and AspF2 from *A. fumigatus* have not only similar properties, but also share 43% of identity upon sequence alignment (Fig. S1†). The same applies to the transmembrane transporter proteins, Zrt1 from *C. albicans* and ZrfC from *A. fumigatus* – 48% sequence identity was observed. The percentage of conserved residues in the two Zn(II) transporting proteins is observed in most other fungi.[22,27]

The aim of this work is to understand the interactions of Zn(II) with Pra1, the *C. albicans* zincophore. We aimed to investigate bioinorganic chemistry of this process, point out the Zn(II) binding sites in Pra1 and understand the thermodynamics of the binding. We use a peptide-based approach, choosing unstructured regions which are most likely to bind zinc and measuring their precise affinity towards zinc ions.

The most common zinc binding sites are quite well described in the literature.[29] The principal ligands that coordinate zinc ions are usually a combination of His, Cys and acidic residues, water molecules and, more rarely, Tyr, Asn, Ser and Thr. The ligand composition and geometry suggest six natural classes: (i) class I, with a ligand group which consists of at least three histidine residues, which share an elongated zinc
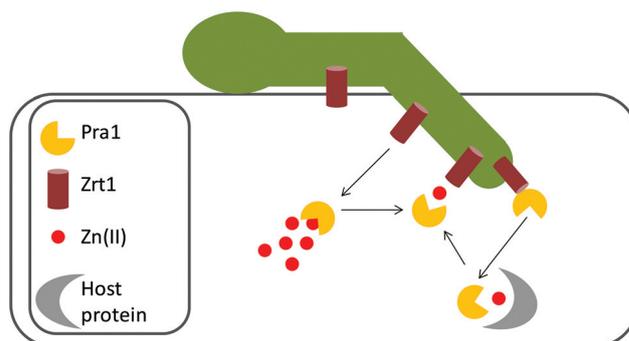
Fig. 1 Schematic model of *C. albicans* zinc scavenging from host cells. After invasion of the host cell, Pra1 is expressed and secreted. It binds zinc, either in the form of free Zn(II) (extremely sparse in the cellular pool) or from zinc-binding proteins of the host reassociation with the *C. albicans* cell surface and Zn(II) transportation into the cell occurs *via* a Pra1–Zrt1 interaction.[22]
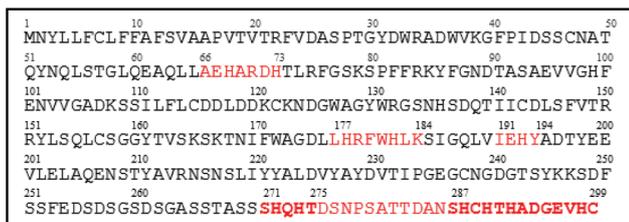
```
 1          10         20         30         40         50
MNYLLFCLFFAFSVAAPVTVTRFVDASPTGYDWRADWVKGFPIDSSCNAT
51         60    66    73         80         90         100
QYNQLSTGLQEAQLLAEHARDHTLRFGSKSPFFRKYFGNDTASAEVVGHF
101        110        120        130        140        150
ENVVGADKSSILFLCDDLDDKCKNDGWAGYWRGSNHSDQTIICDLSFVTR
151        160        170   177      184    191 194    200
RYLSQLCSGGYTVSKSKTNIFWAGDLLHRFWHLKSIGQLVIEHYADTYEE
201        210        220        230        240        250
VLELAQENSTYAVRNSNSLIYYALDVYAYDVTIPGEGCNGDGTSYKKSDF
251        260    271   275        287      299
SSFEDSDSGSDSGASSTASSSHQHTDSNPSATTDANSHCHTHADGEVHC
```

Fig. 2 Amino acid sequence of Pra1; probable Zn(II) binding sites are highlighted in red.

binding motif H̲EXXH̲XXGXXH̲; (ii) class II, which consists of three His, two of which are arranged in a HXH motif, with the third one being in a more distant position; (iii) class III, being a combination of His and Cys residues; (iv) class IV, in which two histidines, one acidic residue and one water molecule are bound to the zinc ion; (v) class V, predominantly acidic ligands; and (vi) other ligand compositions.[22]

As far as the sequence of Pra1 is considered, several zinc binding sites can be found when applying the rules described above (highlighted in red in Fig. 2). Another important issue is the structure of the protein. One of our experimental approaches is based on working with model systems – peptides, which are fragments of Pra1. This approach would not be particularly useful if Pra1 had a pre-defined structure. No crystal or solution structure of Pra1 is available; the structure predicted by Phyre2 (a remote homology recognition technique, able to regularly generate reliable protein models)[30] shows that especially the C-terminal part of the protein is highly unstructured (Fig. S2†) and therefore appropriate for our peptide-based approach.

The protein parts that are studied have carefully been chosen, based on two criteria: (i) being in an unstructured site and (ii) containing the predicted zinc binding sites. To further confirm that the peptides we have chosen are the ones which are most likely to bind Zn(II), we aligned the sequence of Pra1 from *C. albicans* with the sequence of Aspf2 (also important for growth under zinc limitation) from *A. fumigatus* (their sequences share 43% of identity) (Fig. S1†).

The chosen Pra1 fragments include Ac-AEHARDHT-NH₂ (residues 66–73), Ac-LHRFWHLK-NH₂ (residues 177–184), Ac-IEHY-NH₂ (residues 191–194), Ac-SHQHT-NH₂ (residues 271–275), and Ac-SHCHTHADGEVHC (residues 287–299). In addition, a longer fragment, which comprised two of the fragments listed above was studied: Ac-SHQHTDSNPSATTDANSHCHTHADGEVHC (residues 271–299).

Experimental

Synthesis

All peptides (Ac-IEHY-NH₂; Ac-AEHARDH-NH₂; Ac-LHRFWHLK-NH₂; Ac-SHQHT-NH₂; Ac-SHCHTHADGEVHC-COOH; Ac-SHQHTDSNP-SATTDANSHCHTHADGEVHC-COOH) were purchased from KareBayBiochem (USA) (certified purity: 98%)

and were used as received. The carbonate-free stock solution of 0.1 M KOH was purchased from Sigma-Aldrich and then potentiometrically standardized with potassium hydrogen phthalate.

Mass spectrometric measurements

High-resolution mass spectra were obtained on a Bruker MicrOTOF-Q spectrometer (BrukerDaltonik, Bremen, Germany), equipped with an Apollo II electrospray ionization source with an ion funnel. The mass spectrometer was operated both in the positive and in the negative ion mode. The instrumental parameters were as follows: scan range: m/z 300–4000, dry gas: nitrogen, temperature: 170 °C, and ion energy: 5 eV. The capillary voltage was optimized to the highest S/N ratio and it was 4500 V. The small changes of voltage (±500 V) did not significantly affect the optimized spectra. The samples (Zn(II) : ligand in a 1 : 1 stoichiometry, [ligand]$_{tot}$ = 10^{-4} M) were prepared in a 1 : 1 acetonitrile–water mixture at pH 6. The variation of the solvent composition down to 5% of acetonitrile did not change the species composition. The sample was infused at a flow rate of 3 μL min^{-1}. The instrument was calibrated externally with the Tunemix™ mixture (BrukerDaltonik, Germany) in quadratic regression mode. Data were processed using the Bruker Compass DataAnalysis 4.0 program. The mass accuracy for the calibration was better than 5 ppm, enabling together with the true isotopic pattern (using SigmaFit) an unambiguous confirmation of the elemental composition of the obtained complex.

Potentiometric measurements

Stability constants for proton and Zn(II) complexes were calculated from titration curves carried out over the pH range of 2–11 at 298 K and ionic strength 0.1 M (NaClO₄) using a total volume of 3 cm³. The potentiometric titrations were performed using a Dosimat 665 Metrohmtitrator connected to a Metrohm 691 pH-meter and a Metrohm LL Unitrode glass electrode. The thermostabilized glass-cell was equipped with a magnetic stirring system, a microburet delivery tube and an inlet–outlet tube for argon. Solutions were titrated with 0.1 M carbonate-free KOH. The electrodes were calibrated daily for hydrogen ion concentration by titrating HClO₄ with KOH under the same experimental conditions as above. The purities and the exact concentrations of the ligand solutions were determined by the Gran method.[31] The ligand concentration was 0.5 mM and the Zn(II) to ligand ratio was 1 : 1.

The HYPERQUAD 2006 program was used for the stability constant calculations.[32] Standard deviations were computed by using HYPERQUAD 2006 and referenced to random errors only. The constants for hydrolytic Zn(II) species were used in these calculations.[33] The speciation and competition diagrams were computed using the HYSS program.[34]

NMR measurements

NMR spectra were recorded at 14.1 T on a BrukerAvance III 600 MHz equipped with a Silicon Graphics workstation. The temperatures were controlled with an accuracy of ±0.1 K.

Suppression of the residual water signal was achieved by excitation sculpting, using a selective square pulse of 2 ms long on water. All the samples were prepared in a 90% H_2O and 10% D_2O (99.95% from Merck) mixture. Proton resonance assignment was accomplished by 2D ^1H–^1H total correlation spectroscopy (TOCSY) and nuclear Overhauser effect spectroscopy (NOESY) experiments, carried out with standard pulse sequences. Spectral processing and analysis was performed using Bruker TOPSPIN 2.1 and Sparky. The samples of the analyzed complexes were prepared by adding metal ions to an acidic solution of a 3 mM ligand (pH 3), and the pH was then increased to higher values (pH 3.5, 5 and 6).

Results and discussion

In order to provide information about stoichiometry, mass spectrometry was performed. The experiment confirmed that the ligands were pure and proved the formation of the complexes. The stoichiometry of all the studied complexes was 1:1 (metal:ligand ratio). The signals correspond to the equimolar Zn(II) complexes ($m/z = 664.2$, $z = 1+$; $m/z = 520.2$, $z = 2+$; $m/z = 620.3$, $z = 2+$; $m/z = 712.2$, $z = 1+$; $m/z = 513.5$, $z = 3+$; $m/z = 801.3$, $z = 4+$ for the Ac-IEHY-NH$_2$; Ac-AEHARDH-NH$_2$; Ac-LHRFWHLK-NH$_2$; Ac-SHQHT-NH$_2$; Ac-SHCHTH-ADGEVHC-COOH; Ac-SHQHTDSNPSATTDANSHCHTHADGEVHC-COOH, respectively). Peak assignment was compared to simulated isotopic patterns, which fit perfectly to experimental ones (Fig. S3–S8†).

In all measured mass spectra, signals corresponding to sodium and potassium adducts of the ligands are observed. In the case of Ac-IEHY-NH$_2$, a potassium adduct is visible ($m/z = 640.3$, $z = 1+$). The enlarged signal, which corresponds to the zinc complex, also shows small signals which probably are the result of adding one proton to the peptide during ionization (Fig. S3†). In the Zn(II)-Ac-AEHARDH-NH$_2$ mass spectra, potassium adducts of the ligand with one ($m/z = 508.2$, $z = 2+$), two ($m/z = 527.2$, $z = 2+$), three ($m/z = 546.2$, $z = 2+$) and four ($m/z = 565.1$, $z = 2+$) potassium atoms are observed (Fig. S4†). In the Zn(II)-Ac-LHRFWHLK-NH$_2$ mass spectra, beside the signal from the ligand and zinc complex, a ligand adduct with one ($m/z = 608.3$, $z = 2+$) and two potassium atoms ($m/z = 627.3$, $z = 2+$) is visible (Fig. S5†). In the case of Zn(II)-Ac-SHQHT-NH$_2$, sodium ($m/z = 672.3$, $z = 1+$), potassium ($m/z = 688.3$, $z = 1+$) and perchlorate ($m/z = 747.2$, $z = 1+$) adducts of the peptide are present (Fig. S6†). In the Zn(II)-Ac-SHCHTHADGEVHC-COOH mass spectra, a signal which is the result of the loss of a water molecule from the peptide during ionisation ($m/z = 486.2$, $z = 3+$) and a ligand potassium adduct is visible ($m/z = 504.9$, $z = 3+$) (Fig. S7†). In the mass spectra of Zn(II)-Ac-SHQHTDSNPSATTDANSHCHTHADGEVHC-COOH, we observe a signal which comes from the loss of a water molecule from the peptide ($m/z = 781.1$, $z = 4+$), a peptide sodium adduct ($m/z = 791.1$, $z = 4+$), a potassium ligand adduct with one ($m/z = 795.1$, $z = 4+$) and two ($m/z = 804.8$, $z = 4+$) atoms

and a chloride adduct of the zinc complex ($m/z = 810.8$, $z = 4+$) (Fig. S8†).

Protonation of the ligands

The Ac-IEHY-NH$_2$ peptide fragment behaves as an LH$_3$ acid with the deprotonating groups corresponding to the glutamic acid side chain group, and histidine imidazole and tyrosine side chain groups with pK_a values of 4.18, 6.58 and 9.93, respectively. The first two pK_a values of the Ac-AEHARDH-NH$_2$ peptide fragment (3.38 and 4.22) arise from the deprotonation of carboxylic side chain groups of aspartic and glutamic acids and the next two pK_a values (6.25 and 6.97) are related to the deprotonation of two imidazole groups of the histidine residues. The Ac-LHRFWHLK-NH$_2$ peptide fragment acts like a typical LH$_3$ acid. The first two pK_a values (5.83 and 6.59) can be assigned to the deprotonation of two histidine units and the other one (10.29) to the deprotonation of the lysine side chain group. The Ac-SHQHT-NH$_2$ peptide fragment behaves as an LH$_2$ acid with the deprotonating groups corresponding to two histidine imidazole groups with pK_a values of 5.90 and 6.74. The Ac-SHCHTHADGEVHC-COOH and Ac-SHQHTDSNPSATTDANSHCHTHADGEVHC-COOH peptide fragments are C-terminal (shorter and longer) fragments of the Pra1 peptide. In both cases the constants related to the C-terminal carboxylic group were beyond the working range of the electrode. Potentiometric measurements were able to detect eight constants for the Ac-SHCHTHADGEVHC-COOH peptide fragment. The first two acidic constants with pK_a values of 2.95 and 3.90 correspond to aspartic acid and glutamic acid side chain groups. The next four pK_a values (5.07, 6.18, 6.71 and 7.13) arise from the deprotonation of four imidazole groups of histidines and the following two (8.27 and 9.56) come from two cysteine side chain groups. The Ac-SHQHTDSNPSATTDANSHCHTHADGEVHC-COOH peptide fragment has twelve protonation constants. The first three pK_a values (2.85, 2.89, and 3.75) can be assigned to the deprotonation of the carboxylic side chain groups of three aspartic acid residues. The following one with a pK_a value of 4.05 belongs to the deprotonation of a glutamic acid side chain group. The next six constants with pK_a values of 5.05, 6.12, 6.34, 6.75, 7.20 and 7.28 are related to the histidine imidazole groups and the last two (8.36 and 9.71) correspond to two cysteine side chain groups.

Zinc complexes

Zinc coordination to Ac-IEHY-NH$_2$ starts already at pH 3 (Fig. S9†). The first observed form is ZnH$_2$L with a maximum at around pH 5 and involves the glutamic acid in binding. The loss of one proton leads to the ZnHL form, in which the histidine residue is coordinated; this complex dominates near physiological pH (max. at 7.4). At higher pH values, the coordination mode does not change and the loss of two protons is related to the deprotonation of two water molecules bound to the central zinc ion. The last deprotonation corresponds to the deprotonation of the tyrosine side chain, which does not participate in binding.

The first complex observed for Ac-AEHARDH-NH$_2$ is ZnH$_2$L with a maximum at pH 4.5. It involves two acidic residues in binding, which are aspartic and glutamic acids. The next two forms, ZnHL and ZnL, with maxima at pH around 5.8 and 7.3, respectively, are both related to the proton loss and coordination of histidine residues. A significant decrease of the pK_a values calculated for the complexed and free imidazoles (Table 1) suggests that both histidines are involved in zinc binding. The last two observed forms, ZnH$_{-1}$L and ZnH$_{-2}$L, correspond to the deprotonation of two water molecules (Fig. S10†).

In the case of Ac-LHRFWHLK-NH$_2$, zinc coordination starts at pH 3 and the first form we observe is ZnH$_2$L with a maximum at pH 4.6. It involves one histidine imidazole in binding. The next form which dominates at around physiological pH (max. at 7.3) is ZnHL. The lowered pK_a value for the histidine residue in the complexed ligand (5.06) compared to the free one (6.59) implies the participation of this group in binding. The loss of the next two protons leads to ZnH$_{-1}$L, which indicates the proton loss from two water molecules bound to the central zinc atom. The last observed form, ZnH$_{-2}$L, which dominates at basic pH, comes from the deprotonation of lysine, which does not participate in coordination (Fig. S11†). Above pH 9, precipitation of the complex starts to occur.

For Ac-SHQHT-NH$_2$, we observe only two complex forms with zinc ions (Fig. S12†). First of them is ZnL with a maximum at pH 7.0. It engages two histidine residues in binding. The remaining two deprotonations are related to the proton loss of water molecules, which are most probably present in the vacant zinc binding sites.

The first complex form of the C-terminal Ac-SHCHTHADGEVHC-COOH that we observe is ZnH$_3$L with a maximum at around pH 5.6 (Fig. S13†). It involves three histidine residues in binding. Above pH 6, the ZnH$_3$L complex deprotonates to ZnH$_2$L with a pK_a value of 5.94, which corresponds to the remaining histidine residue, which is also involved in coordination (its pK_a in the free ligand = 7.13). The loss of the next two protons corresponds to the deprotonation of two cysteine residues, which do not participate in binding.

The longest examined Pra1 region, Ac-SHQHTDSNPSA-TTDANSHCHTHADGEVHC-COOH, involves the Ac-SHQHT-NH$_2$ and Ac-SHCHTHADGEVHC-COOH fragments. Zinc coordination starts at pH around 4 and the first form, ZnH$_6$L (with a maximum at pH 5.2, Fig. S14†), involves two histidine residues in binding. Around pH 6, the ZnH$_4$L form dominates in solution, with the other two histidine imidazoles being bound to the metal, which by now has a {4N} binding mode. The next two deprotonations with pK_a values of 6.55 and 6.63, respectively (corresponding to two deprotonations of unbound histidines), lead to the formation of ZnH$_3$L and ZnH$_2$L forms. The {4N} binding mode does not change in the two last complex forms, ZnHL and ZnL; deprotonations come from the cysteine side chains which, as in the case of the Ac-SHCHTHADGEVHC-COOH fragment, do not take part in coordination.

Establishing which of the six histidines are bound to the metal was not a trivial task, and it seems quite likely that several species with the same stoichiometry but different donor atom sets are present in solution at the same time and at equilibrium with each other.

NMR measurements were performed in order to point out which imidazoles are involved in binding. NOESY and TOCSY experiments were performed at pH 5 and 6 in the presence as well as in the absence of zinc. The histidine Hα–Hβ and aromatic proton correlations are severely overlapped, most likely because the chemical environment around the histidines is very similar (repetitions of 'SH' and 'HT'). Because of this, we were not able to univocally assign signals coming from each histidine. However, the informative part of the spectra was the region of histidine Hβ–Hδ correlations, which broaden to the baseline upon the addition of zinc. Fig. S15† shows that four such correlations are not affected at pH 5 (maximum abundance of ZnH$_4$L species) and two are still visible at pH 6 (maximum of ZnH$_2$L) (Fig. S16†), confirming the information from potentiometric data – two of the six histidines from this fragment bind Zn(II) at pH 5, and four imidazoles are coordinated at pH 6. Again – which ones? There is virtually no difference in the TOCSY spectra of the discussed fragment recorded with and without the presence of zinc, apart from a partial broadening in the region of the overlapped His Hα–Hβ region at around 3.3–4.7 ppm and the broadening of a small resonance at 2.1–4.3 ppm which can be assigned to the Hα–Hβ correlation of Val297, present only before the last His298 in the studied sequence (Fig. S17†). Naturally, this does not imply the engagement of Val297 in coordination, rather the involvement of His298; the resonances of Val297 are affected due to the fact that they sense a different chemical environment after the binding of Zn(II) to His298, which is in close proximity. The hypothesis that the last four C-terminal His residues are involved in the binding is further supported by a competition plot shown in Fig. 3. The plot is based on the calculated constants, showing a hypothetical situation, in which equimolar amounts of Zn(II), Ac-SHQHTDSNPSATTDANSHCHTHADGEVHC-COOH, Ac-SHCHTHADGEVHC-COOH and Ac-SHQHT-NH$_2$ are present. The comparison of these stabilities shows that the N-terminal part of Ac-SHQHTDSNPSATTDANSHCHTHADGEVHC-COOH-Ac-SHQHT-NH$_2$ is not as effective in binding Zn(II) as the C-terminal Ac-SHCHTHADGEVHC-COOH part. The zinc coordination to Ac-SHCHTHADGEVHC-COOH and Ac-SHQHTDSNPSATTDANSHCHTHADGEVHC-COOH is almost identical until pH 6 – at this point, both complexes have a {4N} binding mode. Above pH 6, Ac-SHQHTDSNPSATTDANSHCHTHADGEVHC-COOH becomes a more efficient Zn(II) binder. We may hypothesize that this is due either to (i) the formation of polymorphic states (species with the same {4N} binding mode but different His imidazole donors are present in solution at the same time and the metal ion can move along the histidines, as described in ref. 35) or to (ii) the protection of the complex core from hydrolysis by non-binding residues that form a set of hydro-

Table 1 Potentiometric data for proton and Zn(II) complexes of Ac-IEHY-NH₂; Ac-AEHARDH-NH₂; Ac-LHRFWHLK-NH₂; Ac-SHQHT-NH2; Ac-SHCHTHADGEVHC-COOH; Ac-SHQHTDSNPSATTDANSHCHTHADGEVHC-COOH

Species	Ac-IEHY-NH₂ $\log \beta$	Ac-IEHY-NH₂ pKa	Ac-AEHARDH-NH₂ $\log \beta$	Ac-AEHARDH-NH₂ pK_a	Ac-LHRFWHLK-NH₂ $\log \beta$	Ac-LHRFWHLK-NH₂ pK_a	Ac-SHQHT-NH2 $\log \beta$	Ac-SHQHT-NH2 pK_a	Ac-SHCHTHADGEVHC-COOH $\log \beta$	Ac-SHCHTHADGEVHC-COOH pK_a	Ac-SHQHTDSNPSATTDANSHCHTHADGEVHC-COOH $\log \beta$	Ac-SHQHTDSNPSATTDANSHCHTHADGEVHC-COOH pK_a
HL	9.93 (3)	9.93 (Tyr)	6.97 (5)	6.97 (His)	10.29 (1)	10.29 (Lys)	6.74 (2)	6.74 (His)	9.56 (1)	9.56 (Cys)	9.71 (2)	9.71 (Cys)
H₂L	16.51 (1)	6.58 (His)	13.22 (4	6.25 (His)	16.88 (1)	6.59 (His)	12.63 (1)	5.90 (His)	17.82 (2)	8.27 (Cys)	18.07 (2)	8.36 (Cys)
H₃L	20.69 (1)	4.18 (Glu)	17.44 (3)	4.22 (Glu)	22.71 (2)	5.83 (His)			24.95 (2)	7.13 (His)	25.35 (4)	7.28 (His)
H₄L			20.82 (3)	3.38 (Asp)					31.65 (2)	6.71 (His)	32.55 (4)	7.20 (His)
H₅L									37.83 (2)	6.18 (His)	39.31 (4)	6.75 (His)
H₆L									42.90 (2)	5.07 (His)	45.65 (4)	6.34 (His)
H₇L									46.80 (2)	3.90 (Glu)	51.77 (2)	6.12 (His)
H₈L									49.75 (2)	2.95 (Asp)	56.82 (3)	5.05 (His)
H₉L											60.87 (3)	4.05 (Glu)
H₁₀L											64.63 (3)	3.75 (Asp)
H₁₁L											67.52 (4)	2.89 (Asp)
H₁₂L											70.37 (3)	2.85 (Asp)
Zn²⁺ complexes												
ZnH₆L											49.72 (5)	
ZnH₅L												
ZnH₄L											39.20 (1)	
ZnH₃L									30.78 (1)		32.66 (4)	6.55 (His)
ZnH₂L	19.91 (4)		17.35 (2)		21.53 (2)				24.84 (1)	5.94 (His)	26.03 (3)	6.63 (His)
ZnHL	13.74 (2)	6.17 (His)	12.26 (3)	5.09 (His)	16.47 (2)	5.06			15.90 (4)	8.95 (Cys)	18.57 (3)	7.46 (Cys)
ZnL			5.99 (3)	6.27 (His)			3.82 (4)	3.82 (2His)	5.93 (6)	9.96 (Cys)	9.50 (4)	9.07 (Cys)
ZnH₋₁L	−1.99 (2)		−2.19 (2)	8.18 (H₂O)	−0.78 (5)							
ZnH₋₂L	−11.64 (2)	9.65	−10.69 (6)	8.50 (H₂O)	−10.74 (6)	9.96	−11.96 (3)					
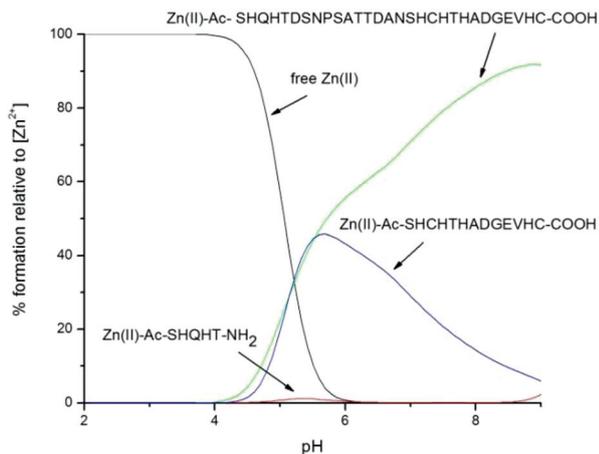
Fig. 3 Competition plot between Pra1 fragments: Ac-SHQHT-NH$_2$, Ac-SHCHTHADGEVHC-COOH, Ac-SHQHTDSNPSATTDANSHCHTHADGEVHC-COOH and Zn(II), describes complex formation at different pH values in a hypothetical situation in which equimolar amounts of the four reagents are mixed. Calculations are based on binding constants from Table 1. Conditions: 298 K, I = 0.1 M, [Zn(II)] = [Ac-SHCHTHADGEVHC-COOH] = [Ac-SHQHTDSNPSATTDANSHCHTHADGEVHC-COOH] = [Ac-SHQHT-NH$_2$] = 0.001 M.
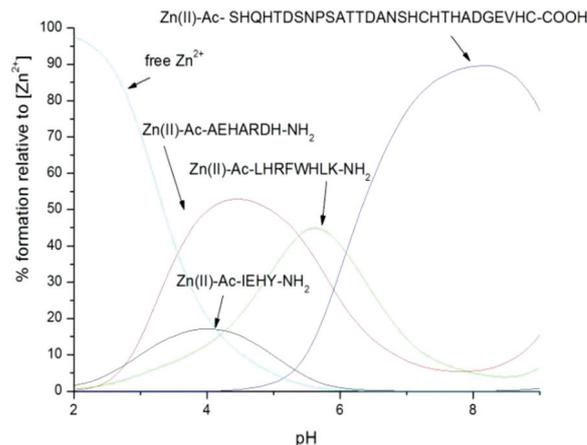
Fig. 4 A competition plot between Pra1 fragments: Ac-IEHY-NH$_2$; Ac-AEHARDH-NH$_2$; Ac-SHQHT-NH$_2$; Ac-SHCHTHADGEVHC-COOH and Zn(II), describes complex formation at different pH values in a hypothetical situation in which equimolar amounts of the four reagents are mixed. Calculations are based on binding constants from Table 1. Conditions: 298 K, I = 0.1 M, [Zn(II)] = [Ac-IEHY-NH$_2$] = [Ac-AEHARDH-NH$_2$] = [Ac-SHQHT-NH$_2$] = [Ac-SHCHTHADGEVHC-COOH] = 0.001M.

gen bonds around the primary coordination sphere (as reported in ref. 36).

Zinc binding site in Pra1

In order to estimate the most probable zinc binding site in Pra1, we used the thermodynamic data for zinc complexes to simulate a theoretical simulation, in which equimolar concentrations of Zn(II) and all the studied unstructured Pra1 fragments were mixed. This allows a direct comparison of the calculated constants at different pH values (Fig. 4).

At acidic pH, fragments with glutamic and/or aspartic acid residues become the anchoring site for Zn(II). It is not surprising that Ac-AEHARDH-NH$_2$, in which two acidic binding groups participate in binding, is preferred over Ac-IEHY-NH$_2$, with only one acidic binding group.

Interestingly, the Ac-LHRFWHLK-NH$_2$ region, in which two histidine residues are the primary zinc binding sites, starts to coordinate already at pH above 3 (*ca.* 3% of available zinc is bound to the sequence). The binding was confirmed by NMR (Fig. S18,† an overlay of TOCSY spectra recorded for the fragment in the presence and absence of Zn(II) at pH 3.5 shows selective broadening of aromatic His protons). In fact, Ac-LHRFWHLK-NH$_2$ is the region of choice for Zn(II) at a narrow pH range from 5.4–6.0. This high affinity towards zinc can be explained by the presence of hydrophobic residues (2 × Leu, Phe, Trp) in close proximity to the binding site. Such an enhancement of zinc binding affinity in the presence of hydrophobic residues was previously observed for carbonic anhydrase[37] or several transcription factors.[38]

Above pH 6, the C-terminal, unstructured Pra1 fragment becomes the primary zinc binding site. At around physiological pH (7.4), more than 85% of the metal is coordinated to this

sequence, being bound to the imidazole nitrogens of His288, His290, His292 and His298. The proposed coordination mode is depicted in Fig. 5.

Previous biological studies have shown that Pra1 is a pH-regulated antigen (PRA1 is transcriptionally upregulated at neutral-alkaline pH).[23] Fig. 4 further confirms the observations made by Citiulo[22] and Wilson[27] that Pra1's recently described role as a zincophore may also be restricted to the environments of higher pH – Pra1's most efficient zinc binding site coordinates the metal with the highest affinity above pH 7.

Pra1's C-terminal affinity for zinc can also be expressed in terms of affinity constants. Based on the concentrations of the ligand, Zn(II) and the formed complex at pH 7.4 from the simulated speciation in Hyss[34] give a 13 nM constant, comparable to that of calprotectin reported by Kehl-Fie.[40] We may hypothesise that Pra1 could compete with calprotectin for the binding of Zn(II), making the zincophore-calprotectin struggle for this metal highly interesting in the field of host–pathogen interactions and nutritional immunity.

The fact that Pra1's C-terminal domain is the most probable Zn(II) binding site is also interesting from an evolutionary perspective[27] – it seems that this binding site is ancient, present not only in ascomycota, but also in basidiomycetes and chytrids (*e.g.* the related C-terminal sequence from *Ustilago maydis* (corn smut fungus, basidiomycete) shares 57.7% identity with the C-terminus studied herein).

The interactions of this biologically crucial region of the Pra1 zincophore, responsible for zinc coordination, with Zrt1, the *C. albicans* surface zinc transporter, will be the subject of further studies.

From a chemical point of view, the obtained data allow a very precise comparison of complex thermodynamics, but how biologically relevant is it? It is obvious, that the placement of
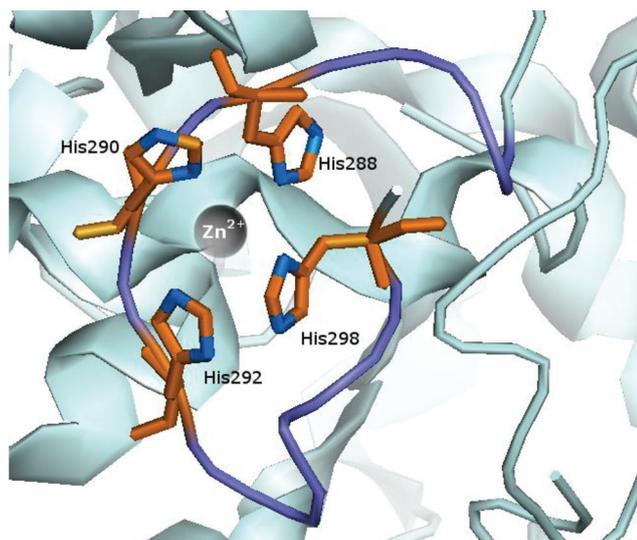
A
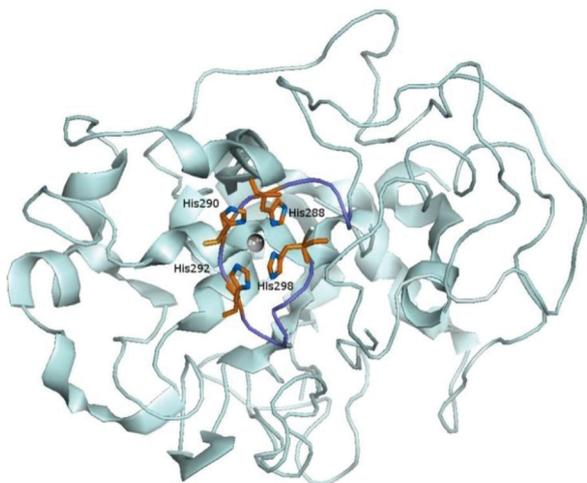
B

Fig. 5 Proposed binding mode for the Zn(II)−Pra1 complex at pH 7.2: (A) view of the whole zincophore; (B) enlarged binding site. Pra1 structure is based on coordinates simulated by Phyre2.[28] The figure was generated using PyMOL.[39]

the studied fragments inside a bigger protein, as well as the presence of the protein in the 'crowded' environment of the host plasma, has an influence on zinc binding, which might turn out to differ moderately from the one calculated in our *in vitro* environment of the chosen peptide fragments. However, the careful choice of fragments for this study based on the criteria of (i) being a good zinc binder; (ii) homology with a zincophore from another fungal species (*A. fumigatus* Aspf2) and (iii) being in an unstructured region of the protein, and therefore appropriate for our peptide-based approach, make this study a biologically relevant one.

Conclusions

Zinc is crucial for the virulence and survival of *C. albicans* in humans. The newly discovered sequestration mode of this element *via* the peptide-based Zn(II) chelating Pra1 zincophore might open new therapeutic possibilities, once the basic bio-inorganic chemistry of this molecule is understood. It is pointed out that the most probable zinc binding site is the first step of the process. Among the precisely chosen, most probable Zn(II) binding sites in Pra1, the unstructured C-terminal region of Pra1 binds Zn(II) with the highest affinity *via* a set of four histidine imidazoles (His288, His290, His292, and His298). This is also the site which will most likely interact with the Zrt1 zinc transporter.

Acknowledgements

References

1 T. Kourkoumpetis, D. Manolakaki, G. Velmahos, Y. Chang, H. B. Alam, M. M. De Moya, E. A. Sailhamer and E. Mylonakis, *Virulence*, 2010, **1**, 359–366.

2 B. J. Kullberg, M. C. Arendrup and E. W. Campion, *N. Engl. J. Med.*, 2015, **373**, 1445–1456.

3 D. W. Denning, A. Pleuvry and D. C. Cole, *Eur. Respir. J.*, 2013, **41**, 621–629.

4 A. L. Mavor, S. Thewes and B. Hube, *Curr. Drug Targets*, 2005, **6**, 863–874.

5 K. Bush, *et al.*, *Nat. Rev. Microbiol.*, 2011, **9**, 894.

6 J. Watly, S. Potocki and M. Rowinska-Zyrek, *Chemistry*, 2016, **22**, 15992–16010.

7 C. Andreini, I. Bertini, G. Cavallaro, G. L. Holliday and J. M. Thornton, *JBIC, J. Biol. Inorg. Chem.*, 2008, **13**, 1205–1218.

8 C. Andreini, I. Bertini and A. Rosato, *Acc. Chem. Res.*, 2009, **42**(10), 1471–1479.

9 S. MacPherson, M. Larochelle and B. Turcotte, *Microbiol. Mol. Biol. Rev.*, 2006, **70**, 583–604.

10 C. S. Hwang, G. E. Rhie, J. H. Oh, W. K. Huh, H. S. Yim and S. O. Kang, *Microbiology*, 2002, **148**, 3705–3713.

11 I. Yike, *Mycopathologia*, 2011, **171**, 299–323.

12 M. Monod, O. Jousson and U. Reichard, in *Aspergillus fumigatus and aspergillosis*, ed. J.-P. Latge and W.J. Steinbach, ASM Press, Washington, DC, 2009, pp. 87–106.

13 T. H. Hyun, E. Barrett-Connor and D. B. Milne, *Am. J. Clin. Nutr.*, 2004, **80**, 715–721.

14 N. W. Tietz and N. M. Logan, *Textbook of Clinical Chemistry*, Saunders, Philadelphia, PA, 1986, p. 1850.

15 I. Bremner and P. M. May, Systemic Interactions of Zinc, in *Zinc in Human Biology. ILSI Human Nutrition Reviews*, ed. C. F. Mills, Springer, London, 1989, pp. 95–108.

16 T. E. Kehl-Fie and E. P. Skaar, *Curr. Opin. Chem. Biol.*, 2010, **14**, 218–224.

17 A. Crawford and D. Wilson, *FEMS Yeast Res.*, 2015, **15**(7), fov071.

18 J. Goyette and C. L. Geczy, *Amino Acids*, 2011, **41**, 821–842.

19 S. S. Mambula, E. R. Simons, R. Hastey, M. E. Selsted and S. M. Levitz, *Infect. Immun.*, 2000, **68**, 6257–6264.

20 C. F. Urban, D. Ermert, M. Schmid, U. Abu-Abed, C. Goosmann, W. Nacken, V. Brinkmann, P. R. Jungblut and A. Zychlinsky, *PLoS Pathog.*, 2009, **5**(10), e1000639.

21 P. K. Walencik, J. Watly and M. Rowinska-Zyrek, *Curr. Med. Chem.*, 2016, **23**, 3717–3729.

22 F. Citiulo, I. D. Jacobsen, P. Miramon, L. Schild, S. Brunke, P. Zipfel, M. Brock, B. Hube and D. Wilson, *PLoS Pathog.*, 2012, **8**, e1002777.

23 M. Sentandreu, M. V. Elorza, R. Sentandreu and W. A. Fonzi, *J. Bacteriol.*, 1998, **180**, 282–289.

24 C. E. Outten and T. V. O'Halloran, *Science*, 2001, **292**, 2488–2492.

25 K. Zakikhany, J. R. Naglik, A. Schmidt-Westhausen, G. Holland, M. Schaller and B. Hube, *Cell. Microbiol.*, 2007, **9**, 2938–2954.

26 J. Amich, R. Vicentefranqueira, F. Leal and J. A. Calera, *Eukaryotic Cell*, 2010, **9**, 424–437.

27 D. Wilson, *Metallomics*, 2015, **7**, 979.

28 J. Amich, R. Vicentefranqueira, E. Mellado, A. Ruiz-Carmuega, F. Leal and J. A. Calera, *Cell. Microbiol.*, 2014, **16**, 548–564.

29 S. Karlin and Z. Y. Zhu, *Proc. Natl. Acad. Sci. U. S. A.*, 1997, **94**, 14231–14236.

30 L. Kelley, PHYRE2 Protein Fold Recognition Server, http://www.sbg.bio.ic.ac.uk/phyre2.

31 G. Gran, *Acta Chem. Scand.*, 1950, **4**, 559.

32 P. Gans, A. Sabatini and A. Vacca, *J. Chem. Soc., Dalton Trans.*, 1985, 1195.

33 L. Pettit and H. K. J. Powell, *The IUPAC Stability Constants Database*, IUPAC, London, 1992–2002.

34 L. Alderighi, P. Gans, A. Ienco, D. Peters, A. Sabatini and A. Vacca, *Coord. Chem. Rev.*, 1999, **184**, 311.

35 J. Watly, E. Simonovsky, R. Wieczorek, N. A. Barbosa, Y. Miller and H. Kozlowski, *Inorg. Chem.*, 2014, **53**, 6675–6683.

36 N. M. Chiera, M. Rowinska-Zyrek, R. Wieczorek, R. Guerrini, D. Witkowska, M. Remelli and H. Kozlowski, *Metallomics*, 2013, **5**, 214–221.

37 J. A. Hunt, M. Ahmed and C. A. Fierke, *Biochemistry*, 1999, **38**(28), 9054–9062.

38 J. M. Berg, *Proc. Natl. Acad. Sci. U. S. A.*, 1988, **85**(1), 99–102.

39 *The PyMOL Molecular Graphics System, Version 1.8*, Schrödinger, LLC.

40 T. E. Kehl-Fie, S. Chitayat, M. Indriati Hood, S. Damo, N. Restrepo, C. Garcia, K. A. Munro, W. J. Chazin and E. P. Skaar, *Cell Host Microbe*, 2011, **10**(2), 158–164, ISSN 1931-3128.